Numerical analysis

RVWWKHuHFWVDUHSURSHUWLHRPR JHQLWD'VTXUH HQRVXH ZWK OHQWK /is FRQVLGHUHG RQLQ7KHOHIWDOORW wall at temperature, T_h, and the right wall is a cold one at temperature, T_c. The upper and lower sides are assumed to be adiabatic. The emissivities of the four DOOVDORKRQQWKHJH

To simplify the problem, some assumptions are HPSOR\HGLQWKLVZN7KHÀXLGFRQVLGHUHGWREH OPLQDUFRPSUHVLEOHDQGWHDG7KHÀXLGZ WRQQQGYLVFRXVDWRQXHOHFWHG7KHÀX is gray with isotropic scattering, and the properties of WKHÀXLGFRQWDQWH[FHSWWKHGHQVLWQGFDWWHUQJ albedo, &The density is assumed to be a linear func tion of temperature. Two cases of inhomogeneity for the scattering albedo are considered in this study:

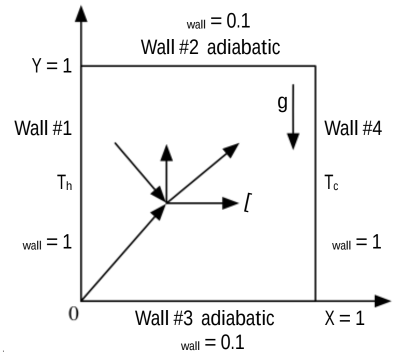

Figure 1. Schematic of computational domain

$$\text{Case A} \quad \frac{1}{\;} \; \frac{3}{Z} \tag{1}$$

$$\text{Case B} \quad Z \;\; 1 \;\; \frac{3}{T}$$

It is assumed that &is a linear function of temperature increases with temperature LQ&DVHDQGGHFUHDVHVZLWKWHPSHUDWXUHLQ&DVH%7KHYDULDWLRQRILQKRPRJHQHLW\LV important factor in this topic. However, past studies only focused on the inhomogeneity due to spatial variation and neglected the dependence of radiative properties on temperature. This WHPSHUDWXUHGHSHQGHQFHHuHFWLVWKHPDLQIRFXVRIWKLVZRUN

The governing equations include continuity, momentum, and energy equations. The GLPHQVLRQOHVVIRUPRIWKHVHHTXDWLRQVDUHZULWWHQDV

– continuity equation

$$\frac{U}{X} \frac{w V}{w Y} \;\; 0 \tag{3}$$

– momentum equation

$$U \frac{U}{X} \; V \frac{w\, U}{w\, Y} \quad \frac{Pw}{Xw} \; \text{Pr} \left(\frac{U}{X} \; \frac{w\, U}{w\, Y} \right)$$

$$U \frac{V}{X} \; V \frac{w\, V}{w\, Y} \quad \frac{Pw}{Yw} \; \text{Pr} \left(\frac{V}{X} \; \frac{w\, V}{w\, Y} \right) \; \text{Ra}\,\text{Pr}\,T \tag{5}$$

where U and VDUHWKHPHQVLRQOHVVYHORFLWLHVLQDQGGLUHFWLRQVUHVSHFWLYHO\LQH QWLRQDOGLHVVLRQOHVVRQDOWULHVVLQHDWLRQDOSUDOVHH

– energy equation

$$U \frac{wT}{X} \; V \frac{wT}{w\, Y} \quad \frac{w\,T}{Xw} \; \frac{T}{Y} \quad \frac{\tau_0\, W T}{\text{Nr}} \; Q_r \tag{6}$$

$$Q_r = \int_{4\pi} I^*(s,\Omega)\Omega \mathrm{d}\Omega \tag{7}$$

In the equations, θ is the dimensionless temperature, θ_0 – the dimensionless temperature ratio, Nr – the conduction-to-radiation parameter, and is an important parameter in the radiative heat transfer problem, and Q_r – the dimensionless radiative heat flux, which can be evaluated from eq. (7) once the radiative intensity is known, and s – the position co-ordinate. The radiative intensity can be obtained by solving the RTE, eq. (8):

– RTE

$$\xi\frac{\partial I^*}{\partial X}+\eta\frac{\partial I^*}{\partial Y}=-\tau I^*+\tau\left[(1-\omega)I_b^*+\frac{\omega}{4\pi}\int_{4\pi} I^*(s,\Omega')\Phi(\Omega',\Omega)\mathrm{d}\Omega'\right] \tag{8}$$

where ξ and η are the directional cosines in x- and y-direction, respectively, I^* – the dimensionless radiative intensity, and I_b^* – the dimensionless blackbody intensity.

The boundary conditions are given in tab. 1.

Table 1. Boundary conditions

	Momentum	Energy
Wall #1	$U = V = 0$	$\theta = 1$
Wall #2	$U = V = 0$	$Q_\mathrm{c} + Q_\mathrm{r} = 0$
Wall #3	$U = V = 0$	$Q_\mathrm{c} + Q_\mathrm{r} = 0$
Wall #4	$U = V = 0$	$\theta = 1$

The dimensionless conduction heat flux can be calculated from:

$$Q_\mathrm{c} = -\frac{Nr}{\theta_0\tau}\nabla\theta \tag{9}$$

The overall local Nusselt number on the hot wall is the sum of the local Nusselt numbers for convection and radiation. The former shows the ratio of convection heat flux to conduction heat flux, the latter shows the ratio of radiation heat flux to conduction heat flux, and they can be calculated from eq. (10).

$$\mathrm{Nu} = \mathrm{Nu}_c + \mathrm{Nu}_r = -\frac{\partial\theta}{\partial X}+\frac{\theta_0\tau}{Nr}Q_r \tag{10}$$

The mean Nusselt number over the hot wall is defined:

$$\overline{\mathrm{Nu}} = \frac{1}{L}\int_0^L \mathrm{Nu}\,\mathrm{d}Y \tag{11}$$

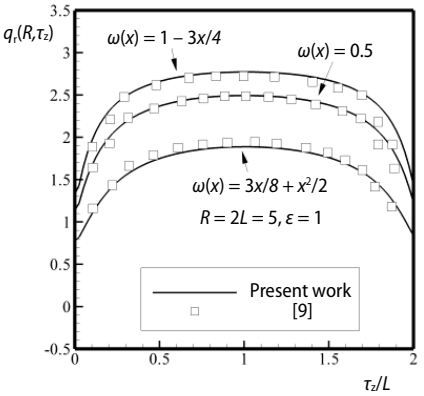

Figure 2. Code verification results

In this work, the RTE is solved using the discrete ordinates method [24], and the continuity, momentum, and energy equations are solved by using the SIMPLE algorithm [25]. Both methods are carried out using Fortran, and the convergence criteria in each calculat-ed variable is set as 10^{-5}. To validate the current code, a 2-D radiation in a cylinder with spatially varying albedo [9] problem is repeated. The radiative flux, q_r, for a hot medium enclosed by cold walls for three albedo distributions are shown in fig. 2 and τ_z is the optical co-ordinate in the z-direction. For all cases, the current results are in very good agreement with the published results. This validates the current computer code.

A grid test is performed to verify the independence of results on the grid size. Because changes in temperature and velocity near boundary in the current problem is larger than that in the central part, a sin-enhanced grid distribution is used in this study. Grid numbers from 112×112 to 142×142 are investigated. Table 2 shows that increasing the grid size from 132×132 to 142×142 results in less than 1% monotonic change in the maximum absolute value of stream function and radiative Nusselt number. Thus 142×142 is chosen for this study.

Table 2. Grid test results; Ra = 10^7, Pr = 1, θ_0 = 1.5, *Nr* = 0.005, τ = 1, Case B

Grid	112×112	122×122	132×132	142×142
$\lvert\psi\rvert_{max}$	349.7	353.7	357.4	360.8
Nu_r	246.4	246.4	246.5	246.5

Table 3. Quadrature scheme test results; Ra = 10^7, Pr = 1, θ_0 = 1.5, *Nr* = 0.005, τ = 1, Case B

Quadrature scheme	S_4	S_6	S_8
$\lvert\psi\rvert_{max}$	360.9	360.8	360.8
Nu_r	246.6	246.5	246.5

Additionally, a S_n quadrature scheme test is also performed. As shown in tab. 3, S_6 quadrature scheme is enough for both energy and momentum calculations, and is used in this study.

Results and discussion

The main purpose of this study is to investigate the effects of inhomogeneity on heat transfer characteristics. Therefore, Prandtl number and the dimensionless temperature ratio, θ_0, are fixed to 1 and 1.5. The controlled variables are Rayleigh number, varying from 10^4 to 10^7, and conduction-to-radiation parameter, *Nr*, varying from 10 to 0.005. In addition, effect of optical thickness is also discussed, with its value varying from 0.1 to 10.

The radiative heat transfer is proportional to the fourth power of temperature. Therefore, it greatly affects the temperature distribution, and also leads to changes in velocity field. The *Nr* is a key dimensionless parameter to describe the strength of radiation, as compared with conduction. As *Nr* decreases, radiation effect increases. Figure 3 shows the temperature distribution for *Nr* = 0.05 for the two cases. In general, the temperature distributions for both cases in this condition are similar. But a further look reveals that the temperature gradient near the hot wall in Case B is larger than that in Case A. Because fluid near the hot wall has a θ value close to 1, therefore the absorption coefficient for Case B is much higher than that in Case A. Energy emitted from the hot wall is more easily absorbed by nearby fluid in Case B.

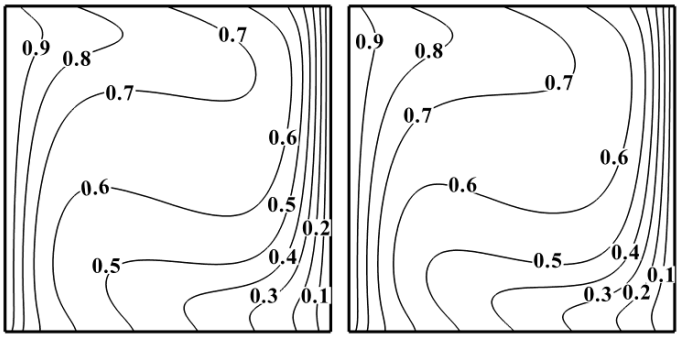

Figure 3. The temperature distribution for Case A (left) and Case B (right) for *Nr* = 0.05; Ra = 10^5, Pr = 1, θ_0 = 1.5, τ = 1

Figure 4 shows the temperature distribution for *Nr* = 0.005. In this condition, *Nr* is small enough so that radiation dominates energy transport in the system. The isotherms in Case B appear to be a diffusion-like process. Again this is due to the highly absorbing ability of the fluid near the hot wall. Energy is absorbed and re-emitted by neighboring fluid, and the process is just like diffusion. As temperature decreasing to the right, isotherms are more and more distorted, and convection effect increases slightly. On the other hand for Case A, absorption is

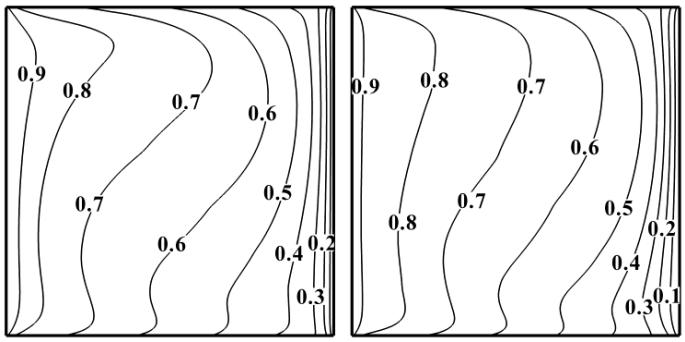

Figure 4. The temperature distribution for Case A (left) and Case B (right) for $Nr = 0.005$; $Ra = 10^5$, $Pr = 1$, $\theta_0 = 1.5$, $\tau = 1$

weaker than in Case B near the hot wall. Thermal energy can penetrate further away from the hot wall and convection effect is more pronounced.

Figures 5 shows the local dimensionless conductive heat flux, Q_c, along the hot wall for different Nr. In these figures, it can be seen that dimensionless conductive heat flux in Case B is always larger than in Case A. As explained previously, thermal energy is more limited to regions close to the hot wall in Case B, so the temperature gradient is larger. Therefore, conductive heat flux is larger in Case B.

In fig. 5(a), it can be noticed that the value of the conductive heat flux is small. For the condition of $Nr = 0.005$, radiation dominates the energy transport and conduction accounts for only 10 to 20 percent of heat transfer. The difference between Case A and Case B is large. When Nr increases to 0.05 and 0.5, as shown in figs. 5(b) and 5(c), the dimensionless conductive heat flux in Case B is still larger than in Case A, but the difference between the two cases becomes smaller. Additionally, it can be found that Q_c is larger near the bottom side ($Y = 0$) than the top side ($Y = 1$). For the condition of $Nr = 0.05$, natural convection is more pronounced. Following the circulation of natural convection, the low-temperature medium is pushed to the bottom side of the hot wall. Temperature gradient is increased and hence the conductive heat flux. For $Nr = 0.5$, as shown in fig. 5(c), the difference of dimensionless conductive heat flux in these cases is still noticeable. It shows that even radiation effect is not the dominant mechanism, the inhomogeneity of the medium still affects the system through the influence of thermal conduction.

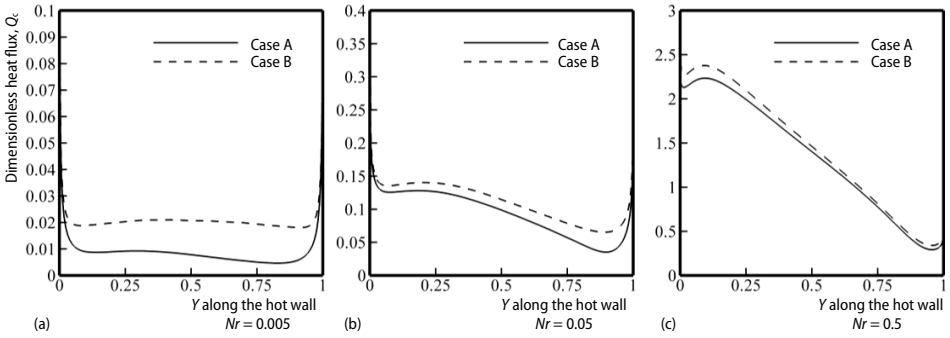

Figure 5. Effects of inhomogeneity of medium on local dimensionless conductive heat flux along the hot wall; $Ra = 10^5$, $Pr = 1$, $\theta_0 = 1.5$, $\tau = 1$

Figure 6 shows the effects of Rayleigh number on dimensionless conductive heat flux for $Nr = 0.05$. As Rayleigh number is increased from 10^4 to 10^7, the conductive heat flux along the hot wall is increased due to the gradual increase of buoyancy force. For $Ra = 10^4$, buoyancy force is not as pronounced, and the difference in conductive heat flux between Cases A and B is obvious. When Rayleigh number is increased to 10^5 and 10^6, buoyance force becomes more pronounced, and the difference caused by the inhomogeneity of medium declines. However, when

Rayleigh number is further increased to 10^7, buoyance force is so strong that large amount of low temperature medium is pushed to the lower side near the hot wall by the strong circulation of natural convection. The local temperature difference is increased, the effect of inhomogeneity is also increased due to the variation of radiative property with temperature. The difference in conductive heat flux between Cases A and B is large, especially at the bottom area along the hot wall.

Figure 7 depicts the effects of inhomogeneity on the maximum absolute value of stream function for different Rayleigh numbers. When *Nr* is small, the difference between Cases A and B becomes more significant. With more energy absorbed at the high temperature area in Case B, the buoyance force in the fluid is enhanced. When *Nr* is larger than 0.05, the flow is less affected by the inhomogeneity of media. On the other hand, when *Nr* is smaller than 0.05, radiation becomes the dominating mechanism of energy transport. More energy is transported into the medium from the hot wall in Case B, and the circulation becomes stronger as evidenced by the higher maximum absolute value of stream function. In addition, the difference in the maximum absolute value of stream function of value of stream function of these two cases increases with the value of Rayleigh number. This is also due to the enhancement of buoyance force in Case B.

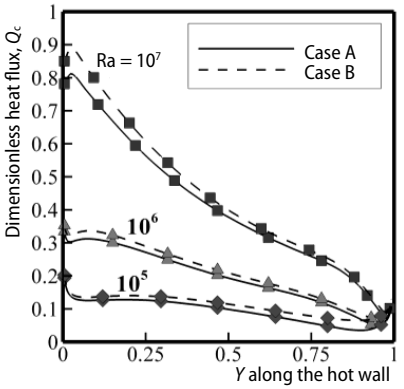

Figure 6. Effects of Rayleigh number on local dimensionless conduction heat flux along the hot wall; *Nr* = 0.05, Pr = 1, $\theta_0 = 1.5$, $\tau = 1$

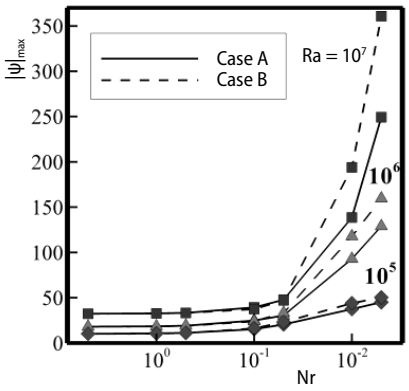

Figure 7. Effects of Rayleigh number on stream function for different *Nr*; Pr = 1, $\theta_0 = 1.5$, and $\tau = 1$

Optical thickness, τ, is a parameter that describes the difficulty that radiation pass through a medium. With larger optical thickness, radiative energy is more likely to be absorbed or scattered by the medium. Figure 8 shows the maximum absolute value of stream function, $|\Psi|_{max}$, *vs.* optical thickness for different Rayleigh numbers. It can be found that $|\Psi|_{max}$ increases with optical thickness. This is because increasing optical thickness makes energy easier to be absorbed or scattered by the medium. The radiative energy is absorbed by the fluid near the hot wall, and natural convection is enhanced. However, the difference in $|\Psi|_{max}$ caused by inhomogeneity of the medium is relatively small for the cases considered.

Figure 9 shows mean Nusselt numbers *vs.* optical thickness for different Rayleigh numbers. Convective Nusselt number increases with Rayleigh number due to stronger buoyancy force. The difference in convective Nusselt number for Cases A and B is quite large. For Case A, Nu_c decreases monotonically with increasing optical thickness. On the other hand, Nu_c for Case B first decreases and then increases with increasing optical thickness. The difference caused by inhomogeneity is small when optical thickness is small because the dif-

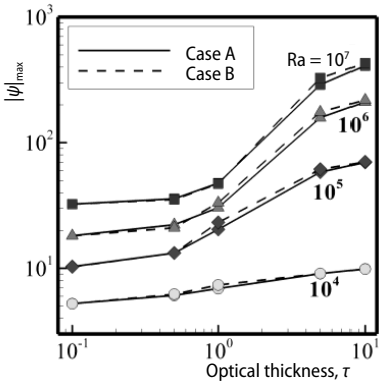

Figure 8. Effects of Rayleigh number on stream function for different optical thickness; Pr = 1, θ_0 = 1.5, and *Nr* = 0.05

ference caused by different radiative transfer mechanism (different albedo value) is small for small τ. The radiation effect becomes obvious when τ is large. The Nu_c for Case A continues to decrease. This is because in Case A, albedo increases with temperature, energy is more likely to be transported to cold region by scattering. Therefore, temperature gradient near the hot wall, and hence Nu_c, decreases. However, for Case B, radiation effect is limited to near the hot wall region when τ is large. A large amount of energy concentrates in the high temperature area. The convection effect is enhanced under these conditions, and hence Nu_c is also increased.

It can also be found in fig. 9 that radiative Nusselt number, Nu_r, increases with increasing τ for all Rayleigh numbers. In the case of strong buoyance force, the temperature distribution is not yet controlled by the radiation mechanism even the optical thickness of the system is large and maintains a vortex shape. The cold medium is moved by the flow motion from the right side and is close to the hot wall, and it leads to a higher radiative energy transfer near the hot wall. Before the radiation mechanism fully dominates the system, a stronger convection would enhance the radiative energy transportation along the hot wall, and it also leads to the result of increasing of radiative Nusselt number.

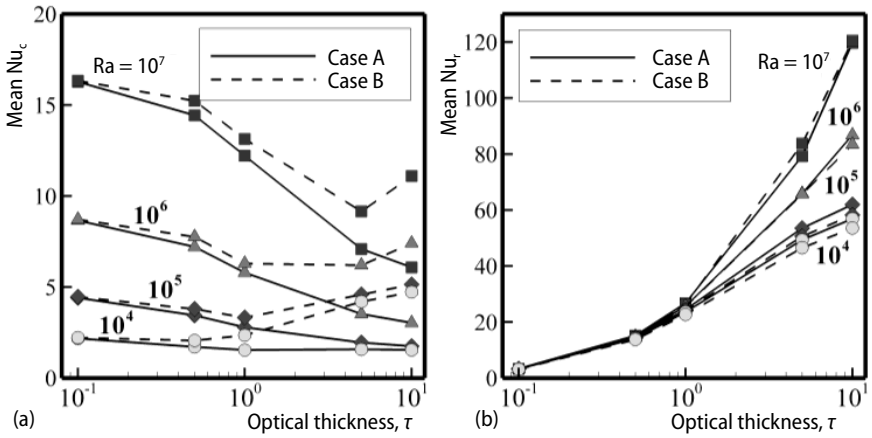

Figure 9. Effects of Rayleigh number on mean convective Nusselt number (a) and radiative Nusselt number (b) of the hot wall for different optical thickness; Pr = 1, θ_0 = 1.5, and *Nr* = 0.05

Conclusions

Effects of radiation on the heat transfer and flow characteristics of an inhomogeneous medium are investigated numerically. Two types of inhomogeneity are considered, and effects of conduction-to-radiation parameter, Rayleigh number, and optical thickness are investigated.

The results show that temperature-dependent properties of the media affect the energy transportation near the hot wall through the change of temperature gradient. For Case B, where the albedo decreases with increasing temperature, radiative transport is more limited to high

[8] Tsai, J. R., Ozisik, M. N., Radiation in Cylindrical Symmetry with Anisotropic Scattering and Variable Properties, *Int. J. Heat Mass Transf., 33* (1990), 12, pp. 2651-2658
[9] Li, H. Y., *et al.*, Two-Dimensional Radiation in a Cylinder with Spatially Varying Albedo, *J. Thermophys. Heat Transf., 6* (1992), 1, pp. 180-182
[10] Farmer, J. T., Howell, J. R., Monte Carlo Prediction of Radiative Heat Transfer in Inhomogeneous, Anisotropic, Nongray Media, *J. Thermophys. Heat Transf., 8* (1994), 1, pp. 133-139
[11] Ruan, L. M., Tan, H. P., Solutions of Radiative Heat Transfer in Three-Dimensional Inhomogeneous, Scattering Media, *Journal of Heat Transfer, 124* (2002), 5, pp. 985-988
[12] Tseng, C.-L., *et al.*, Numerical Analysis of the Solar Reactor Design for a Photoelectrochemical Hydrogen Production System, *Int. J. Hydrogen Energy, 37* (2012), 17, pp. 13053-13059
[13] Ravishankar, M., *et al.*, Application of the Modified Differential Approximation for Radiative Transfer to Arbitrary Geometry, *J. Quant. Spectrosc. Radiat. Transf., 111* (2010), 14, pp. 2052-2069
[14] Muthukumaran, R., *et al.*, Assessment of Signals from a Tissue Phantom Subjected to Radiation Sources of Temporal Spans of the Order of a Nano-, Pico-, and Femto-Second – A Numerical Study, *Numer. Heat Tranf. A-Appl., 60* (2011), 2, pp. 154-170
[15] Chu, H., *et al.*, Calculations of Gas Radiation Heat Transfer in a Two-Dimensional Rectangular Enclosure Using the Line-by-Line Approach and the Statistical Narrow-Band Correlated-k Model, *Int. J. Therm. Sci., 59* (2012), C, pp. 66-74
[16] Jin, Y. Q., An Approach to Two-Dimensional Vector Thermal Radiative Transfer for Spatially Inhomogeneous Random Media, *J. Appl. Phys., 69* (1991), 11, pp. 7594-7600
[17] Meftah, S., *et al.*, Coupled Radiation and Double Diffusive Convection in Nongray Air-CO_2 and Air-H_2O Mixtures in Cooperating Situations, *Numer. Heat Tranf. A-Appl., 56* (2009), 1, pp. 1-19
[18] Moufekkir, F., *et al.*, Combined Double-Diffusive Convection and Radiation in a Square Enclosure Filled with Semitransparent Fluid, *Comput. Fluids, 69* (2012), Oct., pp. 172-178
[19] Moradi, A., Rafiee, R., Analytical Solution to Convection-Radiation of a Continuously Moving Fin with Temperature-Dependent Thermal Conductivity, *Thermal Science*, *17* (2013), 4, pp. 1049-1060
[20] Moradi, A., *et al.*, Convection-Radiation Thermal Analysis of Triangular Porous Fins with Temperature-Dependent Thermal Conductivity by DTM, *Energy Conv. Manag.*, *77* (2014), Jan., pp. 70-77
[21] Sun, Y. S., *et al.*, Application of Collocation Spectral Method for Irregular Convective-Radiative Fins with Temperature-Dependent Internal Heat Generation and Thermal Properties, *Int. J. Thermophys.*, *36* (2015), 10-11, pp. 3133-3152
[22] Edwards, D. K., Radiation Interchange in a Non Gray Enclosure Containing an Isothermal CO_2-N_2 Gas Mixture, *Journal of Heat Transfer, 84* (1962), 1, pp. 1-11
[23] Neuroth, N., Effect of Temperature on Spectral Absorption of Glasses in the Infrared (in German), *Glastechnische Berichte, 25* (1952), pp. 242-249.
[24] Modest, M. F., *Radiative Heat Transfer,* 2nd ed. Academic Press, San Diego, Cal., USA, 2003
[25] Patankar, S. V., *Numerical Heat Transfer and Fluid Flow.* McGraw-Hill, New York, USA, 1980

Paper submitted: February 25, 2016
Paper revised: July 17, 2016
Paper accepted: July 21, 2016